Cold/sticky systems

V. Baglin
CERN, Geneva, Switzerland

Abstract
The understanding of complex and/or large vacuum systems operating at cryogenic temperatures requires a specific knowledge of vacuum science at such temperatures. At room temperature, molecules with a low binding energy to a surface are not pumped. However, at cryogenic temperatures, their sojourn time is significantly increased, thanks to the temperature reduction, which allows a 'cryopumping'. This pumping mechanism is described by different regimes. Sticking probabilities, capture factor and thermal transpiration concepts are also used to characterize the pumping mechanism. At cryogenic temperature, a gas load into a vacuum system turns into an increase of the surface coverage and of its associated vapour pressure. Some adsorption isotherms of H_2 and He which differ with key parameters such as surface nature and temperature are also presented. As an application of this field of vacuum technology, the vacuum system of the CERN Large Hadron Collider is introduced. The implementation of cryosorbers and the consequences of He leaks in the accelerator beam tube are reported.

1 Introduction

At sufficiently low temperature, the vacuum in vessels can be achieved by the adsorption of the molecules due to the attractive van der Waals forces. One of the first applications of the cryopumping mechanism was the realization of storage containers by Sir J. Dewar after the production of liquid hydrogen in the early 1900s [1]. At the end of the 1950s, the early space projects and the requirement for producing large pumping speed in space simulating vacuum chambers at 80 K gave rise to the building of the first large cryopump cooled by helium at $T < 20$ K [2,3]. In the meantime, with the invention of the Gifford–McMahon process [4] used to refrigerate low-noise amplifiers, the modern cryopump was born.

The Large Hadron Collider (LHC) [5], currently under construction at CERN, is one of the world's largest instrument which uses and contributes to the development of the field of vacuum technology at cryogenic temperature. This storage ring will collide protons at 14 TeV in the centre of mass. By means of 8.6 T superconducting dipole magnets operating at 1.9 K, the energetic protons are kept on their circular orbit 26.7 km long. To allow a proper operation of the machine, the beam life time, dominated by the proton scattering on the nucleus of the residual gas, must be greater than 100 h. To fulfil this requirement, the LHC vacuum system has been under careful study and design for more than a decade [6,7].

In Section 2, the main concepts of the cryo-vacuum are described. Sojourn time, regimes of cryopumping, sticking probability, capture factor, and thermal transpiration are discussed and illustrated by examples taken from the literature.

In Section 3, the adsorption isotherms are described in detail. Some models of adsorption isotherms are introduced. The saturated vapour pressure is introduced. Examples of H_2 and He adsorption isotherms are given. The relevance of some parameters such as gas species, temperature, and the porosity of the substrate are supported by data in the literature data.

How the knowledge of vacuum at cryogenic temperature could be applied to the construction of the LHC, particular, the cryosorbers and the helium leaks in the beam vacuum tube are discussed.

Section 4 outlines the principle of the LHC vacuum system with emphasis on the behaviour of the dynamic vacuum in the LHC cryogenic beam pipe. The requirements, the performances and the operation of the cryosorbers to be installed in some of the superconducting magnets of the machine are presented.

Finally, Section 5 discusses the case of the helium leaks in the LHC vacuum tube. A model of the leak propagation is compared with the experimental data. The consequences of the helium leaks, the possible diagnostic means and the remedies are addressed in the context of LHC operation.

2 Cryopumping

2.1 Desorption from a surface

When a molecule is desorbed from a surface at a given activation energy of desorption (or binding energy) E, its rate of desorption is given by the Frenkel equation

$$\frac{\mathrm{d}\theta}{\mathrm{d}t} = -\,\theta\,\nu_0\,e^{-\frac{E}{kT}} \tag{1}$$

where ν_0 is the frequency of vibration of the molecule, k the Boltzmann constant ($86.17 \cdot 10^{-6}$ eV/K), and T the temperature of the surface. The frequency ν_0 is expected to be ~ 10^{13} Hz at room temperature but can increase to ~ 10^{16} Hz for a localized adsorption of a rather immobile molecule. The equation is written for the first-order desorption in which the desorption rate depends linearly on the surface coverage θ. The first-order desorption applies for physisorbed molecules and for non-dissociated chemisorbed molecules (H_2, N_2 and O_2 are dissociatively chemisorbed on metals) [8].

The desorption process is characterized by the sojourn time τ given in Eq. (2). This relation shows that the higher the temperature, the shorter the sojourn time. This fact is routinely observed during a bake-out of a vacuum system when mainly water molecules are desorbed from the surface above 100ºC. Moreover, the equation shows that molecules with low binding energy, i.e., physisorbed molecules, have significant sojourn time at low temperature:

$$\tau = \frac{e^{\frac{E}{k\,T}}}{\nu_0}\ . \tag{2}$$

Table 1 gives some activation energies of desorption of physisorbed (for low surface coverage) and chemisorbed molecules on technical surfaces. The physisorbed molecules have activation energy of desorption in the range of ~0.1 eV and the chemisorbed molecules are in the range of ~1 eV. The activation energy is measured by recording the pressure while the sample's temperature T is increased at a constant rate β, i.e., $T = T_0 + \beta t$ [9]. At the maximum of the desorption rate, i.e., at the pressure peak of the desorption spectrum, the temperature T_P is recorded and the activation energy of the desorption is computed from Eq. (3). This equation is derived from the derivative of (1) which equals zero at the maximum desorption rate:

$$\frac{E}{k\,T_\mathrm{P}^2} = \frac{\nu_0}{\beta} e^{-\frac{E}{kT_\mathrm{P}}}\ . \tag{3}$$

In the case of physisorbed molecules, a significant sojourn time, above 100 h, is obtained for a temperature of the substrate in the range of 5 to 65 K. So, the pumping of most of the gases by

physisorption is achieved below 65 K. A simple cooling of a metallic surface to the liquid nitrogen temperature (77 K) will only pump water molecules.

In an unbaked vacuum system, the residual gas composition is dominated by water which is chemisorbed at room temperature. Indeed, at room temperature, the sojourn time is 100 h for water while it is 3 minutes for hydrogen and more than 6 months for carbon monoxide. Increasing the temperature of the vacuum vessel above 100ºC reduces the sojourn time of water to a minute, and hence strongly reduces the surface coverage and also the outgassing rate of water at room temperature after bake-out. However, molecules which are strongly bounded to the material's surface can be desorbed by stimulated desorption (in an accelerator for instance). Therefore, a bake-out up to at least 300ºC is required to reduce the stimulated desorption of carbon monoxide molecules with 1.7 eV binding energy.

Table 1: Activation energies of desorption *E* of some physisorbed (with low surface coverage) and chemisorbed molecules

Molecule	***E* [eV]**	**Surface**
Physisorbed		
H_2	0.017	Stainless steel 316 L [10]
H_2	0.065	Stainless steel 316 L [10]
H_2	0.081	Saran charcoal [8]
H_2	0.23	Carbon fibre [11]
Chemisorbed		
H_2	0.9	Stainless steel 304 L [12,13]
H_2O	1.1	Aluminium [14]
CO	1.2	Stainless steel 316 L [15]
CO	1.7	Stainless steel 316 L [15]

2.2 Cryopumping regimes

At cryogenic temperature, a molecule interacting with a surface is physisorbed, owing to the Van der Waals force, if the surface is 'cold enough'. Several regimes of cryopumping are defined.

- Physisorption is the regime of the sub-monolayer coverage. The van der Waals force acts between the adsorbed molecule and the material surface. The binding energies are those given in Table 1. For hydrogen, the binding energy varies from 20 to 65 meV for smooth and porous material. One hour sojourn time is obtained at 5 K and 20 K, respectively. Since the binding energy for physisorption is larger than the heat of vaporization (10 meV for hydrogen), sub-monolayer quantities of all gas can be physisorbed in sub-saturated conditions at their boiling temperature. Pumps relying on physisorption are called cryosorption pumps [16].
- As far as the surface coverage increase, the van der Waals force acts between the molecules themselves. This is the cryocondensation regime. While increasing the surface coverage, a saturation equilibrium between gas adsorption and desorption is reached. This is the saturated vapour pressure. The activation energy of desorption equals the energy of vaporization. It ranges from 10 to 175 meV for hydrogen and carbon dioxide, respectively. Cryocondensation is the pumping of gas due to a phase change into a solid or a liquid (i.e., an ice or frost of the gas). Pumps relying on condensation are called cryocondensation pumps [17].

– The possibility to use a condensable gas to trap a non-condensable gas with a high vapour pressure is called cryotrapping. For instance, argon is used to trap helium and hydrogen in cryopumps. The trapped molecules are incorporated in the condensable carrier so that the equilibrium pressure is significantly lower than in pure physisorption.

2.3 Sticking probability, pumping speed, and capture factor

The sticking coefficient for cryosorption and cryocondensation is the ratio of the average number of molecules which stick when impinging on a cold surface divided by the total number of impinging molecules. The sticking coefficient ignores the effects of the vapour pressure. It varies between 0 and 1. The value is a function of the gas species, the surface nature, the surface coverage, the temperature of the gas, and the surface temperature. Figure 1 shows the sticking coefficient of hydrogen at 300 K incident onto a surface at 3.1 K as a function of surface coverage [18]. The sticking coefficient increases with the surface coverage. For thick surface coverage above 10^{17} H_2/cm^2 (~ 100 monolayers), the sticking coefficient approaches unity. It is then named condensation coefficient since the pumping is in the cryocondensation regime. Figure 2 shows the variation of the hydrogen condensation coefficient onto a surface at ~ 4 K for different temperatures (i.e., energies) of the incoming hydrogen [19]. For low energies, the condensation coefficient is close to one. It is still above 0.8 for hydrogen held at room temperature.

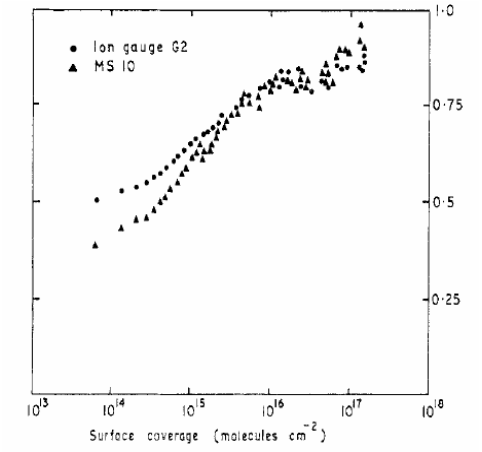

Fig. 1: Sticking coefficient of hydrogen as a function of the surface coverage. The hydrogen is at 300 K incident onto a surface at 3.1 K [18].

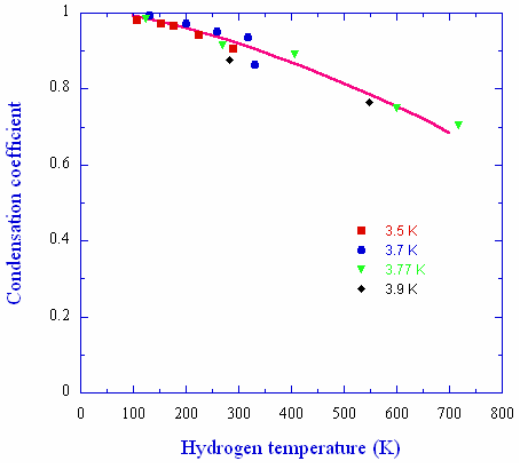

Fig. 2: Hydrogen condensation coefficient onto a surface at ~ 4 K as a function of the hydrogen temperature [19]

Since a cold surface acts as a pump, its pumping speed must be evaluated. If the temperature at the surface of the condensate is so high that the vapour pressure P_{vap} of the solid gas becomes comparable with the pressure of the incident gas P, the pumping speed S of the cryopump is given by Eq. (4) and the effective pumping speed reduces to zero when $P = P_{vap}$. However, most cryopumps do not operate in such conditions so that the pumping speed is simplified to the product of the sticking probability σ times the aperture conductance of the cold surface.

$$S = \frac{1}{4}\sigma\left(1-\frac{P}{P_{vap}}\right)A\overline{V} \approx \frac{1}{4}\sigma\, A\overline{V}\ , \tag{4}$$

where A is the geometrical area of the surface and $\overline{V}$ the mean molecular velocity. A practical formula of the pumping speed in $l \cdot s^{-1} \cdot cm^{-2}$ is given by

$$S = 3.64\sigma\sqrt{\frac{T}{M}} \tag{5}$$

where T is the temperature of the surface (i.e., when the temperature of the gas is accommodated to the surface temperature) and M the molecular weight of the incident gas. At 4.2 K, the maximum pumping speed of hydrogen and carbon monoxide equals 5.3 and 1.4 $l \cdot s^{-1}cm^{-2}$.

In a cryopump, on account of heat load, the cold surface is shielded from the part of the vacuum vessel held at room temperature which must be evacuated. So the molecules must find their way towards the cold surface to be pumped. This geometrical effect is taken into account by the capture probability. The computing of the capture probability is required to optimize the design of the vacuum system. Monte Carlo methods or angular coefficients methods can be used to compute the capture probability. For instance, the cryopump head is shielded from the radiation heat load by chevron-type baffles. In this case, the pumping speed of the cryopump is reduced compared to the pumping speed of the cold surface. The capture probability is estimated to be 0.3 [20,21]. In another example, the angular coefficients method has been used to optimize the position of the holes in the electron shield with respect to the position of the pumping holes in the LHC beam screen [22].

2.4 Thermal transpiration

To reduce the heat load on the cryogenic system, the measurement of a vacuum system held at cryogenic temperature is usually made by vacuum gauges located in a room-temperature vacuum vessel. In this case, a thermal transpiration correction must be applied (the Knudsen relationship) [23]. When two vessels at two different temperatures T_1 and T_2 communicate by a small aperture, the collision rate is conserved when the steady state is established. By equating the fluxes, and since the mean velocity scales like $\sqrt{T}$, the ratios of the pressure P_1/P_2 and the gas density n_1/n_2 in the two vessels are given by

$$\frac{P_1}{P_2} = \sqrt{\frac{T_1}{T_2}} \quad \text{and} \quad \frac{n_1}{n_2} = \sqrt{\frac{T_2}{T_1}} \ . \tag{6}$$

In practice, when measured at room temperature, the pressure inside a vacuum vessel cooled with liquid helium (4.2 K) is the measured pressure divided by 8. The measured pressure must be divided by two for a vacuum vessel cooled with liquid nitrogen (77 K).

Figure 3 demonstrates the validity of the thermal transpiration correction. The figure shows the adsorption isotherms of hydrogen at 4.2 K measured by a gauge located at room temperature and a gauge immersed in liquid helium at 4.2 K [24]. For ease of comparison, the thermal transpiration correction is applied to the gauge located at room temperature. The pressure is therefore given in both cases for a 4.2 K temperature. As expected from the thermal transpiration theory, the values are similar for the two gauges' readings at least over six decades!

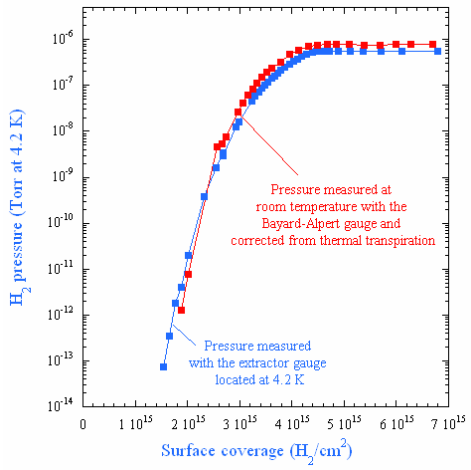

Fig. 3: Adsorption isotherms of H_2 at 4.2 K measured by an ionization gauge located at room temperature and an ionization gauge immersed in liquid helium at 4.2 K [24]

3 Adsorption isotherms

3.1 Some models

The measurement at constant temperature of the equilibrium pressure (vapour pressure) as a function of the surface coverage is the adsorption isotherm. The adsorption isotherm is a function of the molecular species, the temperature of the surface, the nature of the surface, and the gas composition. In the following, some measurements of the isotherms are extracted from the literature to illustrate the effects of the various parameters. The examples are limited to hydrogen and helium since they are the main gases present in a vacuum system at liquid-helium temperature.

There are several semi-empirical adsorption isotherms. At low surface coverage, when there are no lateral interactions between the adsorbed gas molecules, the vapour pressure follows Henry's law. It predicts that the surface coverage θ will vary linearly with pressure P:

$$\theta = cP \ . \tag{7}$$

In the sub-monolayer range, for metallic, glass and porous substrate, the isotherm is better described by the DRK (Dubinin, Raduskevic and Kanager) model. The model is valid at low pressure and offers a good prediction of the isotherm as a function of temperature [25]. The DRK Eq. (8) connects the surface coverage, θ, the monolayer surface coverage, θ_m, the temperature, T, the saturated vapour pressure, P_{sat}, and the pressure, P, via a constant D. A plot of the measured isotherm in the DRK coordinates, i.e., $\ln(\theta)$ vs. ε^2, yields a straight line from which the constant D and the monolayer capacity can be computed:

$$\ln(\theta) = \ln(\theta_m) - D\varepsilon^2 = \ln(\theta_m) - D\left[kT\ln\left(\frac{P_{sat}}{P}\right)\right]^2 \ . \tag{8}$$

The BET (Brunauer, Emmet and Teller) is a multimonolayer description of the isotherm. It links the surface coverage, θ, the monolayer surface coverage, θ_m, the saturated vapour pressure, P_{sat}, and the pressure, P, with a constant α. The constant α is much larger than one so the BET Eq. (9) is simplified. Again, from the measured isotherm, the monolayer capacity can be computed from a linear plot in the BET coordinates $P/[\theta(P - P_{sat})]$ vs. P/P_{sat}. It should be noted that the monolayer surface coverage derived by the BET model is different from the one derived by the DRK model. Despite this, the model covers the entire pressure range from Henry's law to the saturated vapour pressure of the adsorbate; it is only an adequate description of the experimental data in the range $0.01 < P/P_{sat} < 0.3$ [26]:

$$\frac{P}{\theta\,(P - P_{sat})} = \frac{1}{\alpha\theta_m} + \frac{(\alpha - 1)}{\alpha\theta_m}\frac{P}{P_{sat}} \approx \frac{1}{\theta_m}\frac{P}{P_{sat}} \ . \tag{9}$$

3.2 Saturated vapour pressure

The saturated vapour pressure of the gases is the pressure of this gas over its liquid or its gas phase, i.e., when many monolayers of gas are condensed. The saturated vapour pressure follows the Clausius–Clapeyron equation (A and B are constant):

$$\mathrm{Log}(P_{sat}) = A - \frac{B}{T} \ . \tag{10}$$

Figure 4 shows the saturated vapour pressure of the most common gases as a function of temperature [8]. The pressures, corrected from the thermal transpiration, are at room temperature. The figure indicates that below 20 K, the saturated vapour pressures of most of the gases are below 10^{-13} Torr. Therefore, large quantities of such gases can be pumped below 20 K. At liquid-helium

temperature, 4.2 K, only helium and hydrogen are not pumped. At 4.2 K, the saturated vapour pressure of hydrogen is ~ 10^{-6} Torr as already shown in Fig. 3.

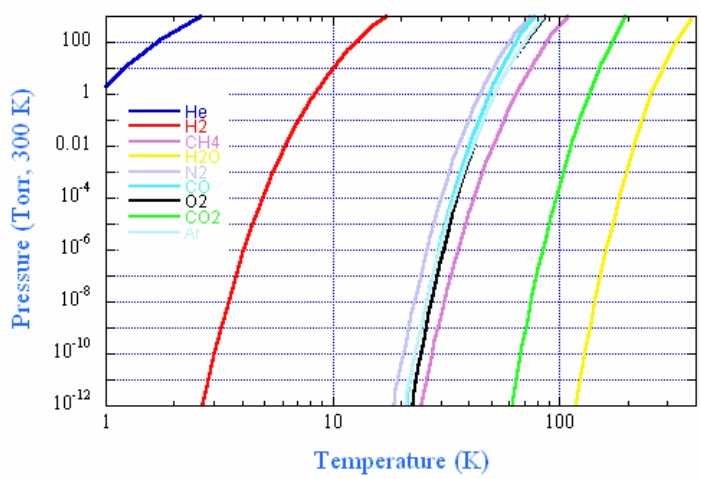

Fig. 4: Saturated vapour pressure curves as a function of temperature [8]

3.3 Hydrogen adsorption isotherms

By pumping on a liquid helium bath, the temperature of the liquid helium can be reduced to allow the pumping of large quantities of hydrogen with a condensation cryopump [27]. The condensation cryopump which operated from 2.3 K (50 Torr on the helium bath) to 4.2 K (atmospheric pressure) can be used to measure the adsorption isotherm of hydrogen as a function of temperature [28].

Figure 5 shows the adsorption isotherm of hydrogen onto a stainless steel surface as a function of temperature. The monolayer capacity is estimated to be $3 \cdot 10^{15}$ H_2/cm^2. Below 3 K, the saturated vapour pressure of hydrogen is negligible. Above 10^{16} H_2/cm^2 the saturated vapour pressure is reached. The results follow the Clausius–Clapeyron law illustrated in Fig. 4 and expand over five decades.

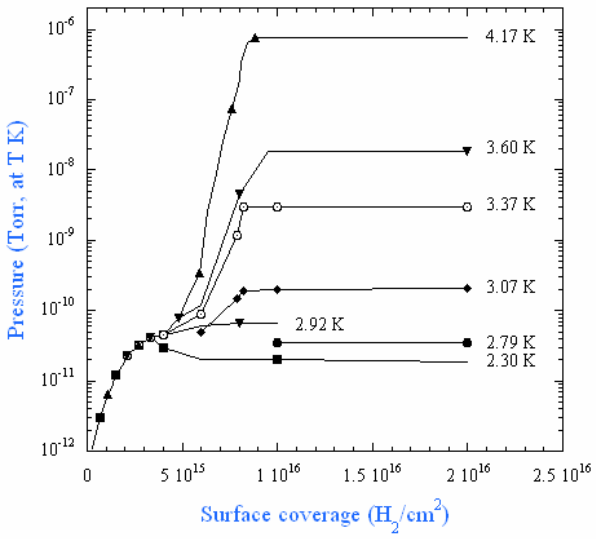

Fig. 5: Hydrogen adsorption isotherm onto a stainless steel surface as a function of the temperature [28]

The addition of a gas can drastically change the shape of the hydrogen isotherm [29]. For example, a frost of carbon dioxide, which is condensed onto the surface prior to the hydrogen injection, forms a porous layer. As shown in Fig. 6, the adsorption capacity of the electroplated Cu

surface is increased. The steep pressure rise is shifted from $2 \cdot 10^{15}$ to $6 \cdot 10^{15}$ H_2/cm_2 due to the carbon dioxide frost. The estimated DRK adsorption capacity of the condensate is 0.3 H_2/CO_2. Similarly, the admission of gas in the vacuum chamber might change the appearance of the adsorption isotherm. This is again the case of carbon dioxide mixed with hydrogen. As shown in Fig. 7, injecting a mixture of 45% H_2 and 55% CO_2 decreases the level of the saturated vapour pressure by 2 orders of magnitude. This phenomenon is applied in cryopumps when carbon dioxide is injected to enhance the pumping of hydrogen and helium by cryotrapping.

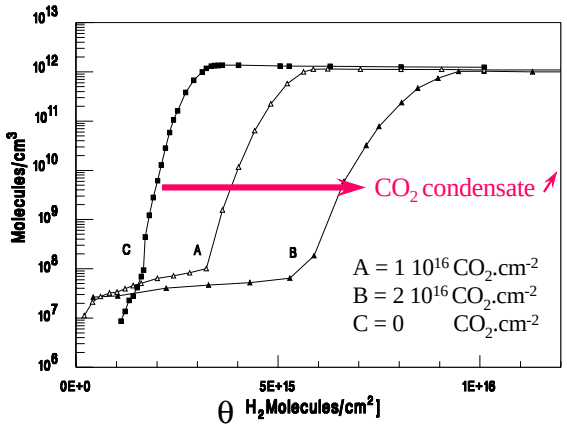

Fig. 6: H_2 adsorption isotherm at 4.2 K on a precondensed layer of CO_2 [29]

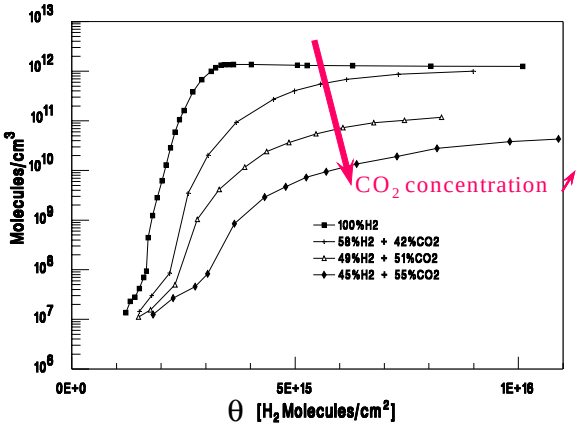

Fig. 7: H_2 co-adsorption isotherm at 4.2 K with CO_2 [29]

3.4 Helium adsorption isotherm

Another gas of interest at cryogenic temperature is helium. As shown by the saturated vapour pressure of helium in Fig. 4, one must operate below 4 K to obtain a low vapour pressure of helium. So, if one wants to perform measurements in UHV condition, one must work in the sub-monolayer range. Thus this is a good test of the validity of Henry's law. Figure 8 shows the helium adsorption isotherm on a stainless-steel tube as a function of temperature [30]. As expected, the isotherms are well described by the DRK model with $\theta_m = 1.3 \cdot 10^{15}$ H_2/cm^2 and $D = 2.92 \cdot 10^4$ eV^{-2}. Below 10^{-9} Torr, the isotherms start to approach the behaviour of Henry's law.

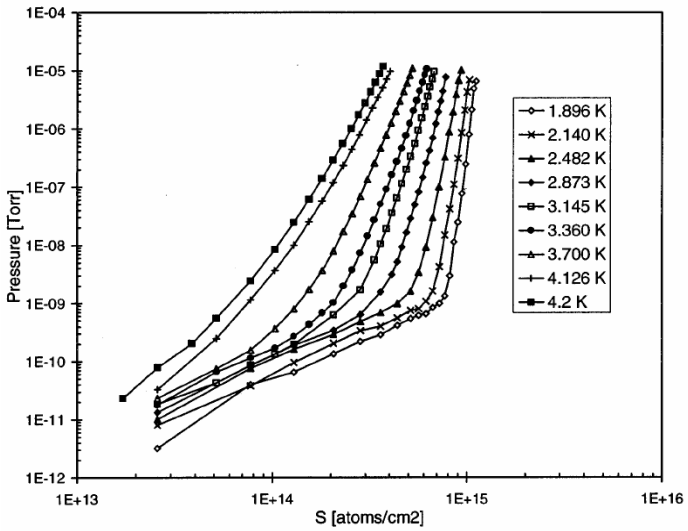

Fig. 8: Helium adsorption isotherm measured on a stainless-steel tube from 1.9 to 4.2 K [30]

3.5 Roughness factor

With the exception of the hydrogen condensation at low temperature, the hydrogen and helium capacities on technical metallic surface are very small, i.e., 10^{14} to 10^{15} molecules/cm^2. Cryosorbing materials are used to increase the capacity, the pumping speed, and the operating range of temperature of vacuum pumps. For instance: activated charcoal is used in cryosorption pumps. Its capacity is ~ 10^{22} H_2/g, i.e., 10^{21} monolayers [8]. Its sticking probability equals 0.3 at 30 K [31]. Thanks to these properties, activated charcoal is mounted onto cryopanels installed at the second stage of a cryopump to allow the pumping of hydrogen and helium at 20 K [16].

The capacity of cryopanels is usually measured with the BET method. From the xenon isotherm at 77 K, the BET monolayer θ_m is obtained. Since the area of the xenon molecules is about 25 Å^2, the roughness factor, i.e., the ratio of the real surface over the geometrical surface is computed. Table **2** shows the roughness factor of several technical surfaces. Metallic surfaces have roughness factors close to unity, i.e., a low surface capacity whereas porous surfaces such as anodized aluminium and Non Evaporable Getter (NEG) St 707 have large roughness factors [32].

Table 2: Roughness factor of some technical surfaces

Technical surface	Unbaked	Baked at 150ºC
Copper Cu-DHP acid etched	1.4	1.9
Stainless steel 304 L vacuum fired	1.3	1.5 (at 300ºC)
Aluminium degreased	3.5	3.5
Sealed anodized aluminium 12 V	24.9	Not measured
Unsealed anodized aluminium 12 V	537.5	556.0
NEG St 707	70.3	156.3

3.6 Carbon fibre cryosorber

Usually cryopanels of cryopumps are made of activated coconut charcoal. In some circumstances and for technological reasons, this material cannot be used. This is the case of the cryosorbers of the LHC which are made of woven carbon fibre due to installation and radiation issues [33]. This cryosorber has the appearance of a fabric with woven carbon fibre. A carbon fibre wire is ~ 1 mm diameter. The wires are woven. The fibres that compose the wire are ~ 10 μm diameter. Each fibre has pores which range from 50 to 500 nm. The pumping speed and the capacity are provided by the trapping of the molecules within these pores. The performance of the cryosorber is a function of the pore size distribution [10,16,34]. Figure 9 shows the hydrogen adsorption isotherms on a woven carbon fibre [11]. The capacity, which is defined here by the amount of gas which can be pumped with an equilibrium pressure not exceeding the LHC operating pressure, ranges from 10^{18} to 10^{17} H_2/cm^2 at 6 K and 30 K, respectively. The roughness factor of such a cryosorber is about one thousand times larger than a metallic surface. Figure 10 shows the sticking probability of the woven carbon fibre. At 10^{18} H_2/cm^2, the sticking probability decreases from 0.3 to 0.1 at 6 K and 30 K, respectively. The values are comparable with those of the activated charcoal.

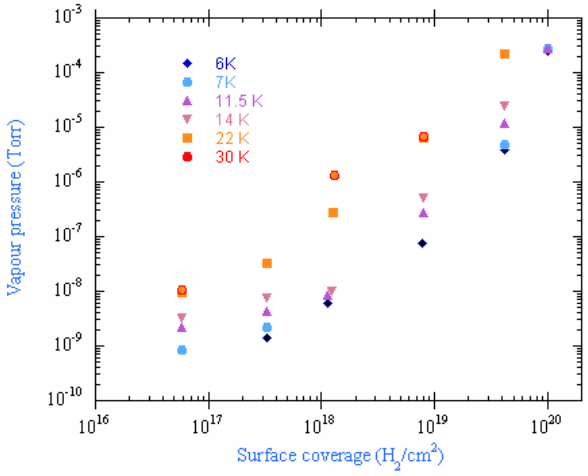

Fig. 9: Hydrogen adsorption isotherms on a woven carbon fibre from 6 K to 30 K [11]

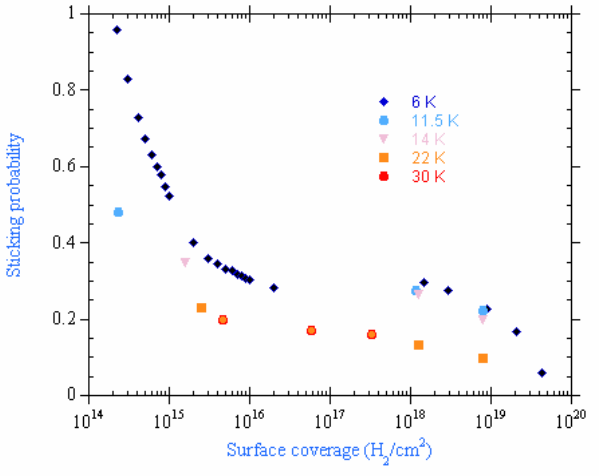

Fig. 10: Sticking probability of the carbon fibre cryosorber, in the 6 K to 30 K temperature range [11]

4 Cryosorbers in cold systems: the case of the LHC superconducting magnets operating at 4.5 K

4.1 LHC arc vacuum system principle

The LHC is a ring of 26.7 km circumference. The ring is divided into eight octants of 2.8 km each. An octant is made of a repetition of cells of superconducting dipoles and quadrupoles. The superconducting magnets operate at 1.9 K. There are eight insertions of 575 m long. The two proton beams of 530 mA and 7 TeV will collide in four of those insertions: the experimental areas.

In the arcs, the vacuum system is made of a cold bore held at 1.9 K surrounded by the superconducting coils assembled in a cold mass. A perforated beam screen operating at 5 K to 20 K is inserted into the cold bore to intercept the thermal loads induced by the circulating beam.

During LHC operation, the proton beams will stimulate molecular desorption by photon, electron and ion bombardment [6,35]. Consequently, the desorbed molecules must be pumped to ensure a beam lifetime of 100 h which is equivalent to a hydrogen pressure of 10^{-8} Torr when measured at room temperature. Figure 11 shows a cross-section of the actively cooled beam screen in the cold bore. The positions of the source of gases are sketched with green arrows. Chemisorbed molecules are desorbed from the beam screen surface by photons, electrons, or ions. These molecules are either physisorbed onto the beam screen surface or pumped through the holes where they are condensed onto the cold bore at 1.9 K. Hydrogen, which has a high vapour pressure (see Fig. 5) cannot be physisorbed in large quantities onto the beam screen and is therefore mainly pumped through the holes. Other molecules, which have low vapour pressure, are physisorbed onto the beam screen. However, scattered photons and electrons can recycle these molecules into the gas phase. When the amount of desorbed molecules is balanced by the amount of physisorbed molecules, an equilibrium pressure and an equilibrium surface coverage are reached [36]. The equilibrium density n_{eq} is driven by the pumping speed of the holes, C, the photon, electron and ion fluxes, $\dot{\Gamma}$, and by the primary desorption yield, η. As a consequence, the LHC vacuum system designer had only to play with the number of holes and the quality of the technical surface to fulfil the design requirements.

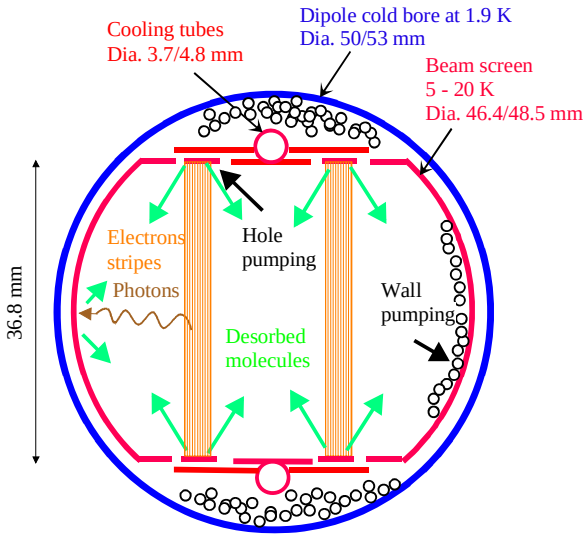

Fig. 11: Cross-section of the LHC vacuum system

$$n_{\mathrm{eq}} = \frac{\eta \dot{\Gamma}}{C} \tag{11}$$

The equilibrium surface coverage on the beam screen θ_{eq} is a function of the monolayer coverage θ_{m} driven by the pumping speed of the beam screen, σS, the holes' pumping speed, C, the primary desorption yield, η, and the recycling desorption η_0' at one monolayer. The equilibrium surface coverage is below a monolayer for low sticking probability and large recycling desorption yield:

$$\theta_{\mathrm{eq}} = \left(\frac{\sigma S}{C} \frac{\eta}{\eta_0'} \right) \theta_{\mathrm{m}} \ . \tag{12}$$

Figure 12 shows the hydrogen dynamic pressure inside a beam screen which is irradiated with synchrotron radiation simulating one third of the LHC design current [37]. The vapour pressure (~ 10^{-10} Torr) is subtracted from the data. Without the pumping holes, the pressure increases due to the recycling desorption by the scattered photons of the physisorbed hydrogen. Since the experimental apparatus has a limited length of 2 m, the hydrogen pressure levels off at 10^{-9} Torr due to the external pumping speed at the extremity. However, if the length had been longer, i.e., in the case of the LHC arcs, the pressure would have continued to increase above the design value. Therefore the beam screen must be perforated to allow the pumping of the recycled hydrogen towards the cold bore. When perforated with 2% holes, the hydrogen pressure levels off at $4 \cdot 10^{-10}$ Torr a value under the LHC design pressure.

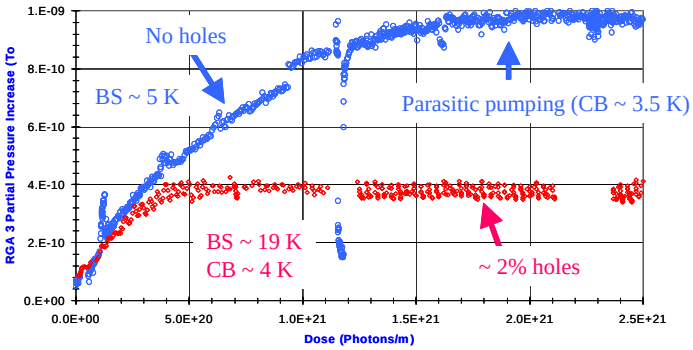

Fig. 12: Comparison of the H_2 photodesorption between a beam screen with and without holes [37]

4.2 LHC long straight sections

In the LHC insertions, the long straight sections, the perforated beam screen technology is still required for cryogenic reasons and for controlling the dynamic vacuum. But, some superconducting magnets operate with a cold bore at 1.9 K and others with a cold bore at 4.5 K. The cumulated length represents 660 m at 1.9 K and 740 m at 4.5 K. The vacuum system of the magnets operating at 1.9 K will behave as described in Section 4.1. However, the long-term operation of the LHC desorbs several monolayers of hydrogen. So, as shown in Figs. 4 and 5, the saturated vapour pressure will be negligible at 1.9 K but will be several orders of magnitude above the design pressure at 4.5 K. Therefore the vacuum system of the magnets operating at 4.5 K requires the insertion of a cryosorber to fulfil the vacuum requirements.

Figure 13 shows a picture of such a beam screen with a cryosorber. In the coaxial space between the beam screen and the cold bore an electron shield is clamped onto the cooling capillary. This electron shield is installed to protect the cold bore from the heat load dissipated by an electron cloud. The cryosorber is a black ribbon installed between the beam screen and the electron shield. By this means, 200 cm^2/m of cryosorber is installed in the narrow space between the beam screen and the cold bore. The chosen cryosorber for the LHC is woven carbon fibre [33].

The vacuum requirements for the LHC cryosorber are the following:

- Installed outside the beam screen in the shadow of the proton beam
- Operation from 5 K to 20 K
- Capacity larger than 10^{18} H_2/cm^2
- Capture coefficient larger than 15%

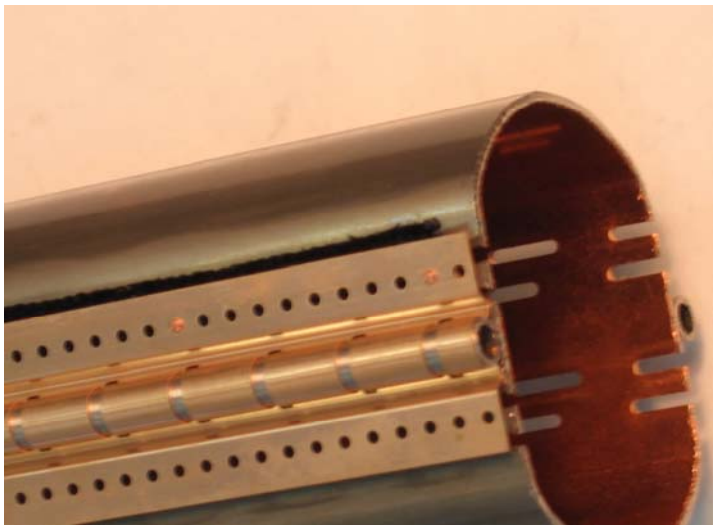

Fig. 13: Photograph of a beam screen equipped with a cryosorber inserted in superconducting magnets operating at 4.5 K

The principle of operation with the cryosorber was checked in a dedicated set-up [38]. In this experiment, the cryosorber was activated charcoal. To study the dynamic vacuum, a beam screen was irradiated with synchrotron radiation while the cold bore was held at 70 K. An equivalent of ~ 100 monolayers of H_2 desorbed from the beam screen was condensed onto the cryosorber prior to irradiation. Under stimulated photodesorption, the hydrogen pressure remains below the LHC design pressure while the beam screen temperature was in the range 15 K to 20 K. So, for a gas load twenty times larger than the design capacity, the cryosorber could maintain the required vacuum performances.

In the LHC, the cryosorbers are installed on the back of the beam screen to provide the required capacity and pumping speed for H_2. These cryosorbers are located in the superconducting magnets operating with a cold bore at 4.5 K. During the annual shutdown, a regeneration of the cryosorber is required. The cryosorber is regenerated at about 80 K. During the regeneration, the beams must not circulate and the beam screen must be warmed up to more than 80 K while the cold bore is held at more than 20 K. This action is required to empty the cold masses. While the hydrogen is desorbed from the cryosorber, it will be evacuated from the vacuum system by the mobile turbomolecular group. This manipulation is expected to last no more than a few days [39].

5 Helium leaks in cold systems: the LHC beam tube case

The LHC operates with superfluid helium at 1.9 K. Several thousand welds are made to assemble the different components of the LHC for its construction. During the design phase, the materials were carefully selected and special care was taken to eliminate welds between UHV vessels and liquid helium vessels. By design, full penetration welds are forbidden along the beam screen cooling capillaries. All the beam screens are leak checked before their insertion into the superconducting magnets. Thus the occurrence of a helium leak in the LHC beam vacuum system is minimized.

If a helium leaks appears in the beam tube held at 1.9 K, the gas is physisorbed locally before any possible detection. As a consequence, pressure bumps, radiation dose and even magnet quench (a transition from the superconducting to the resistive state of the magnet) might appear during machine operation. So, the estimation of the pressure evolution due to helium leaks is of great importance [40,41].

When a helium leak appears, a pressure wave develops with time along the beam vacuum chamber [42]. The He condenses onto the 1.9 K surface up to a monolayer. For larger surface coverage, the He pressure increases to the saturated vapour pressure (2261 Pa). With time, the helium accumulates and the helium wave can span over several tens of metres without being detected. Consequently, the local pressure bump yields to a local proton loss and a risk of quench.

Figure 14 shows a typical evolution with time of the helium pressure wave along the cold bore axis. The helium leak is located at $x = 0$. At $t = 0$, the pressure at the level of the leak, P_{XF}, is simply defined by the ratio of the leak rate Q to the pumping speed of the cold bore aperture. As time goes on, the cold bore is saturated with helium and the effective pumping speed at the level of the leak is decreased. As a result, the pressure at the level of the leak increases. The pressure profile along the cold bore is linear. At $t1$, the pressure at the level of the leak equals $P_{0,t1}$ and the pressure at the level of the front wave [$x = X_F(t1)$] is P_{XF}. At a larger time $t2$ the pressure at the level of the leak has increased and the helium wave arrives at $X_F(t2)$.

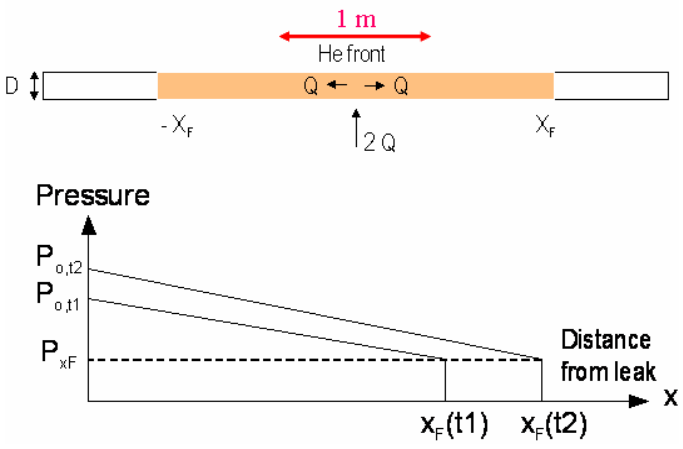

Fig. 14: Evolution of helium pressure with time along the cold bore axis

A model of the helium propagation wave was developed during the design of the Relativistic Heavy Ion Collider (RHIC) and is used for the LHC case [42]. This model of the He propagation wave was validated in a dedicated experiment performed in the LHC test string in a LHC type cold bore at 1.9 K [43]. Figure 15 shows the evolution of the pressure measured at the level of the leak (almost flat curve) and the pressure measured 73.5 m downstream from the leak. The predictions of the model are superimposed on the original data. The green curve is the predicted pressure at the leak and the orange curve is the predicted pressure 73.5 m downstream from the leak. The pressure is given at 1.9 K. At $t = 0$, a leak of $6 \cdot 10^{-5}$ Torr · l/s at room temperature is admitted into the system. It is interesting to observe that for such a leak rate the pressure at the level of the leak is 10^{-6} Torr corresponding to 10^{-5} Torr at room temperature. Therefore, after less than a few minutes, if a proton beam at 7 TeV had interacted with such a gas density, the superconducting magnets would have quenched. However, despite this large leak rate, the helium signal is observed 73.5 m downstream to the leak only 20 h after the opening of the leak. The model predicts the appearance of the leak signal after 17 h which is in good agreement with the observations.

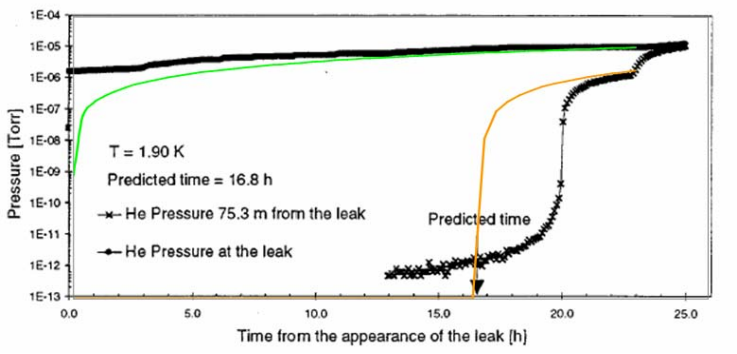

Fig. 15: Example of the evolution with time of a He pressure front observed in the LHC string experiment [43]. The predictions of the model are superimposed on the original data.

At 7 TeV, $8 \cdot 10^{6}$ protons/m/s provoke a magnet quench. So, when the amount of proton losses, due to the nuclear scattering on the helium gas in the vicinity of the leak, approaches this number, the quench of the superconducting magnet is triggered. It can be shown that a helium leak rate above $5 \cdot 10^{-7}$ Torr · l/s must be detected to avoid the risk of a magnet quench. Lower leak rates can be handled by pumping the beam tube each year but, for instance, a leak rate larger than 10^{-5} Torr · l/s triggers a quench within a day. So, the detection of a potential helium leak is of great importance.

In the LHC arc, the minimum distance between two consecutive vacuum gauges is 150 m. This distance is too large to allow a diagnostic of a leak before a quench occurs. So, other means of diagnostics are required. The beam-loss monitors might be used to detect leak rates below 10^{-6} Torr · l/s. The measurement of the dissipated power in the cold masses sounds a realistic means of diagnostic. If 1 W/m can be measured, this cryogenic diagnostic would allow one to detect leak rates up to 10^{-5} Torr · l/s.

In all cases, if a leak is suspected in a given area, an intervention in the tunnel will allow the diagnostic to be improved. When possible, the cold mass temperature must be increased to 4 K to shift the helium front towards the closest short straight section where a vacuum port is located. Afterwards, a residual gas analyser must be installed to perform the leak detection. If the leak needs to be monitored during the beam operation, mobile radiation monitors can be installed to follow the radiation wave associated with the pressure wave [44].

When a magnet has already quenched, it is identified by the triggered diode. During the quench, the cold bore of the magnet is warmed up to more than 30–40 K. So, the helium in the beam tube, if responsible for the quench, is flushed to the nearest unquenched magnet and condensed over a few metres. Again, helium leak detection must be done with a residual gas analyser.

The repair of a leaking magnet is considered in the following way. For a small helium leak rate, a regular warm-up of the cold bore above 4 K and a pump-out of the helium every month allows the machine to operate with a reduced beam current. The time estimate to perform such a job is one day. For larger leak rates, an exchange of the magnet must be foreseen. However, before doing such work, more time must be invested to be sure that the observed quench is indeed due to a helium leak. For this reason, it is imperative that helium has been clearly identified with a residual gas analyser. Moreover, the position of the leak and its rate must be known.

6 Summary

The understanding of the vacuum at cryogenic temperature is required to design and operate large vacuum systems held at cryogenic temperature. Vacuum at cryogenic temperature is encountered in many domains. The areas of fusion technology, space technology, cryogenic technology, and accelerator technology have driven many developments. A few basic concepts and the knowledge required to enter the field of vacuum at cryogenic temperature are recalled in the text. The interaction of a gas molecule with a surface at cryogenic temperature is mainly described by the pumping speed and the adsorption isotherm. These quantities are a function of several parameters: temperature, gas species, etc. In this paper, the characteristics of a cryosorber and of helium have been chosen to illustrate the consequences on the design phase and the operation phase of the LHC vacuum system. First, the insertion of the carbon fibre cryosorber ensures the vacuum performance of the superconducting magnets operating at 4.5 K. Second, in the case of helium leaks, the understanding of the behaviour of the helium gas in the 1.9 K beam tube is mandatory to optimize the exploitation of the LHC.

Acknowledgements

I am indebted to O. Gröbner and the late A.G. Mathewson who led me to the field of vacuum at cryogenic temperature. It is my pleasure also to thank my colleagues of the CERN vacuum group for their support and expertise, with a special credit to B. Jenninger for his technical skills and enthusiasm. The organizers of the school are gratefully acknowledged for having given me the opportunity to present this lecture at the CERN Accelerator School.

Books

The Physical Basis of Ultrahigh Vacuum, P.A. Redhead, J.P. Hobson and E.V. Kornelsen (Chapman and Hall, London, 1968).

Capture Pumping Technology, K.M. Welch (North-Holland, Amsterdam, 2001).

Cryopumping: Theory and Practice, R.A. Haeffer (Oxford Science Publications, Oxford, 1989).

Physical Adsorption of Gases, D.M. Young and A.D. Crowell (Butterworths, London, 1962).

Vacuum Technology, A. Roth (North-Holland, Amsterdam, 1990).

Scientific Foundations of Vacuum Techniques, A. Dushman and J.M. Laferty (John Wiley & Sons, New York, 1962).

References

[1] J. Dewar, *Collected Papers* (Cambridge University Press, 1927).

[2] B.M. Bailey and R.L. Chuang, *Trans. Nat. Vac. Symp.* **5** (1958) 262.

[3] B.G. Lazarev, Je.S. Borovik, M.F. Fedorova and N.M. Zin, *Ukr. Phys. J.* (1957) 176.

[4] W.E. Gifford and H.O. McMahon, *Adv. Cryog. Eng*. **5** (1960) 354.

[5] LHC Design Report, Edited by O. Brüning, P. Collier, P. Lebrun, S. Myers, R. Ostojic, J. Poole and P. Proudlock, CERN-2004-003, 2004, CERN, Geneva, Switzerland.

[6] A.G. Mathewson, Vacuum technology for superconducting colliders, *Proc. of the 15th Particle Accelerator Conf.* (PAC'93), May 1993, Washington, DC, USA.

[7] O. Gröbner, Overview of the LHC vacuum system, *Vacuum* **60** (2001) 25.

[8] P.A. Redhead, J.P. Hobson and E.V. Kornelsen, *The Physical Basis of Ultrahigh Vacuum* (Chapman and Hall, London, 1968).

[9] P.A. Redhead, Thermal desorption of gases, *Vacuum* **12** (1962) 203.

[10] G. Moulard, B. Jenninger and Y. Saito, Industrial surfaces behaviour related to the adsorption and desorption of hydrogen at cryogenic temperature in the LHC vacuum system, *Vacuum* **60** (2001) 43.

[11] V. Baglin, H. Dupont and T. Garcin, Vacuum characterisation of a woven carbon fiber cryosorber in presence of H_2, *Proc. of the 9th European Particle Accelerator Conf.* (EPAC'04), 2004, Luzern, Switzerland.

[12] S. Rezaie-Serej and R.A. Outlaw, Thermal desorption of CO and H_2 from degassed 304 and 347 stainless steel, *J. Vac. Sci. Technol., A* **12** (1994) 2814.

[13] J-P. Bacher, C. Benvenuti, P. Chiggiato, M-P. Reinert, S. Sgobba and A.-M. Brass, Thermal desorption study of selected austenitic stainless steels, *J. Vac. Sci. Technol., A* 167 (2003) **21**.

[14] M. Mohri, S. Maeda, H. Odagiri, M. Hashiba, T. Yamashina and H. Ishimaru, Surface study of type 6063 aluminium alloys for vacuum chamber materials, *Vacuum* **34** (1984) 643.

[15] A. Mathewson, R. Calder, A. Grillot and P. Verbeek, Thermal desorption of CO from some stainless steels, *Proc. 7th Intern. Vac. Congr. & 3rd Intern. Conf. Solid Surfaces*, Vienna, 1977.

[16] Ch. Day, Cryopumping – basics and applications, these proceedings.

[17] C. Benvenuti, Characteristics, advantages, and possible applications of condensation cryopumping. *J. Vac. Sci. Technol.*, **11** (1974) 591.

[18] J.N. Chubb, L. Gowland and I.E. Pollard, Condensation pumping of hydrogen and deuterium on to liquid-helium-cooled surfaces, *J. Phys., D* **1** (1968) 361.

[19] J.N. Chubb and I.E. Pollard, Experimental studies of hydrogen condensation on to liquid helium cooled surfaces, *Vacuum* **15** (1965) 491.

[20] C. Benvenuti and D. Blechschmidt, The optimization of a tubular condensation cryopump for pressures below 10^{-13} Torr, *Proc. Of the 6th Int. Vacuum Congr.*, Kyoto, 1974, *Jpn. J. Appl. Phys.* **2** (1974) 77.

[21] R.A. Haefer, Cryogenic vacuum techniques, *J. Phys., E* **14** (1981) 273.

[22] A.A. Krasnov, Molecular pumping properties of the LHC arc beam pipe and effective secondary electron emission from Cu surface with artificial roughness, *Vacuum* **73** (2004) 195.

[23] A. Dushman and J.M. Laferty, *Scientific Foundations of Vacuum Techniques* (John Wiley & sons, New York, 1962).

[24] V. Baglin. A. Grillot and A.G. Mathewson, Fonctionnement d'une jauge à ionisation à la température de l'helium liquide, Vacuum Technical note 95-01, January 1995, CERN, Geneva, Switzerland.

[25] J.P. Hobson, Physical adsorption isotherms extending from ultrahigh vacuum to vapour pressure, *J. Phys. Chem.* **73** (1969) 2720.

[26] J.P. Hobson, Analysis of ultrahigh vacuum isotherm data with the Brunauer–Emmett–Teller Equation, *J. Vac. Sci. Technol., A* **14** (1996) 1277.

[27] C. Benvenuti, Characteristics, advantages, and possible applications of condensation cryopumping, *J. Vac. Sci. Technol.* **11** (1974) 591.

[28] C. Benvenuti, R.S. Calder and G. Passardi, Influence of thermal radiation on the vapour pressure of condensed hydrogen (and isotopes) between 2 and 4.5 K, *J. Vac. Sci. Technol.* **13** (1976) 1172.

[29] E. Wallén, Adsorption isotherms of H_2 and mixtures of H_2, CH_4, CO, and CO_2 on copper plated stainless steel at 4.2 K, *J. Vac. Sci. Technol., A* **14** (1996) 2916.

[30] E. Wallén, Adsorption isotherms of He and H_2 at liquid He temperatures, *J. Vac. Sci. Technol. A* **15** (1997) 265.

[31] T. Satake, M. Hashiba, M. Mohri and Y. Yamashina, A fundamental study of cryopumping systems with charcoal sorption panel, *Fus. Tech.* **6** (1984) 511.

[32] V. Baglin, Mesure de la rugosité de surfaces techniques à l'aide de la méthode BET, Vacuum Technical note 97-03, January 1997, CERN, Geneva, Switzerland.

[33] V.V. Anashin, I.R. Collins, R.V. Dostovalov, Z.A. Korotaeva, A.A. Krasnov, O.B. Malyshev and V.A. Poluboyarov, Vacuum performance of a carbon fibre cryosorber for the LHC LSS beam screen, *Vacuum* **75** (2004) 293.

[34] D.W. Sedgley, A.G. Tobin, T.H. Batzer and W.R. Call, Characterisation of charcoals for helium cryopumping in fusion devices, *J. Vac. Sci. Technol., A* **5** (1987) 2572.

[35] N. Hilleret, Non-thermal outgassing, these proceedings.

[36] V.V Anashin, G. Derevyankin, V.G. Dudnikov, O.B. Malyshev, V.N. Osipov, C.L. Foerster, F.M. Jacobsen, M.W. Ruckman, M. Strongin, R. Kersevan, I.L. Maslennikov, W.C. Turner and W.A. Lanford, Cold beam tube photodesorption and related experiments for the Superconducting Super Collider Laboratory 20 TeV proton collider, *J. Vac. Sci. Technol., A* **12** (1994) 1663.

[37] V. Baglin, I.R. Collins, O. Gröbner, C. Grünhagel and B. Jenninger, First results from COLDEX applicable to the LHC cryogenic vacuum system, *Proc. of the 7th European Particle Accelerator Conf.* (EPAC'00), 2000, Vienna, Austria.

[38] V. Baglin, I.R. Collins, O. Gröbner, C. Grünhagel and B. Jenninger, Crysorber studies for the LHC long straight section beam screens with COLDEX, *Proc. of the 8th European Particle Accelerator Conf.* (EPAC'02), 2002, Paris, France.

[39] V. Baglin, Vacuum transients during LHC operation, *Proc. of the LHC Project Workshop* – Chamonix XIII, 2004, CERN-AB-2004-014 ADM, CERN, Geneva, Switzerland.

[40] V. Baglin, How to deal with leaks in the LHC beam vacuum. *Proc. of the LHC Project Workshop* – Chamonix XIV, 2005, CERN-AB-2005-014, CERN, Geneva, Switzerland.

[41] V. Baglin, He leaks in the CERN LHC beam chambers operating at cryogenic temperatures, *Vacuum* **81** (2007) 803.

[42] J.P. Hobson and K.M. Welch, Time-dependent helium and hydrogen pressure profiles in a long, cryogenically cooled tube, pumped at periodic intervals, *J. Vac. Sci. Technol., A* **11** 1566 (1993).

[43] E. Wallén, Experimental test of the propagation of a He pressure front in a long, cryogenically cooled tube, *J. Vac. Sci. Technol., A* **15** (1997) 4949.

[44] V. Talanov, V. Baglin and T. Wijnands, Radiation monitors as a vacuum diagnostic in the room temperature parts of the LHC straight sections, *Proc. of the 10th European Particle Accelerator Conf.* (EPAC'06), 2006, Edinburgh, Scotland.